

Full Length Article

UO₂ dissolution in aqueous halide solutions exposed to ionizing radiationJunyi Li^{a,*}, Xianjie Liu^b, Mats Jonsson^a^a Department of Chemistry, School of Engineering Sciences in Chemistry, Biotechnology and Health, KTH Royal Institute of Technology, SE-10044 Stockholm, Sweden^b Laboratory of Organic Electronics, Department of Science and Technology, Linköping University, Norrköping SE-60174, Sweden

ARTICLE INFO

Keywords:

UO₂
 Studtite
 XPS
 Tribromide ion
 Radiolysis

ABSTRACT

In this work, we have experimentally studied UO₂ dissolution in pure water and in 1 M aqueous solutions of either Cl⁻ or Br⁻ exposed to γ -radiation. It has previously been found that high ionic strength can facilitate adsorption of dissolved UO₂²⁺ on UO₂ surfaces. The adsorption is also affected by the solution pH relative to the point of zero charge of UO₂. In our experiments, Br₃⁻ was observed in 1 M Br⁻ solution exposed to γ -radiation. Experiments confirmed that Br₃⁻ can quantitatively oxidize UO₂. XPS and UPS were used to characterize potential surface modifications after exposure. The XPS results show that the UO₂ surfaces after exposure to γ -radiation in pure water and in 1 M aqueous solutions of either Cl⁻ or Br⁻ were significantly oxidized with U(V) as the dominating state. U 4f_{7/2} and O 1s spectra of the UO₂ surface after exposure to γ -radiation in pure water demonstrates the formation of uranyl peroxide secondary phases. UPS results indicate that there is a large percentage of U(VI) on the ultra-thin outer layer of UO₂ after exposure to γ -radiation in 1 M aqueous solutions of Br⁻ and Cl⁻, and 100 % of U(VI) in the pure water case.

1. Introduction

Nuclear power constitutes a significant part of the energy supply portfolio in many countries. One of the major issues related to nuclear power is how to handle the highly radioactive spent nuclear fuel. Currently, reprocessing or permanent disposal are the only two strategies for handling the spent nuclear fuel. Many countries plan to use deep geological repositories to store the spent nuclear fuel for at least 100,000 years (e.g., Sweden, Finland, UK and Canada,). [1–5] During such long-time frame, groundwater intrusion upon multiple barrier failure is a scenario that has to be addressed in the safety assessment of a deep geological repository. Spent nuclear fuel consists of 95 % UO₂ and 5 % fission products and heavier actinides. In general, the fuel matrix (UO₂) has very low solubility in reducing environment. However, when spent nuclear fuel comes in contact with groundwater, the inherent radioactivity of the fuel will induce the radiolysis of water producing oxidizing (HO•, HOO•, and H₂O₂) as well as reducing (eaq⁻, H•, and H₂) species. [6,7] Since UO₂ cannot be further reduced in aqueous phase, the oxidants will dominate the surface reactions and oxidize the U(IV) to U(VI). The latter releases as uranyl (UO₂²⁺) in aqueous system and can coordinate with Lewis base ligands such as H₂O, CO₃²⁻, OH⁻, O₂²⁻, and Cl⁻. [8–12] One of the oxidizing species mentioned above, H₂O₂, can react with UO₂²⁺ forming studtite (UO₂O₂·4H₂O), which has been found as a

secondary phase formed on spent nuclear fuel stored in cooling pools. [13,14].

UO₂ may interact with saline waters under certain situations, e.g. when the core of a damaged nuclear reactor is emergency-cooled with sea water (as after the Fukushima nuclear accident.) [14–16] The Cl⁻ concentration in sea water close to Fukushima was reported as 0.6 M. [17] Another situation is when spent nuclear fuel is considered to be placed in a deep geological repository using rock salt as a host rock e.g., as has been applied in USA (Waste Isolation Pilot Plant (WIPP)), an operating geologic repository for disposal of transuranic nuclear waste), and discussed in Germany; or near the coast e.g. in Sweden, Finland, and has been discussed in UK and Canada. [1–4,18,19] The deep groundwater in these sites contains approximately 0.1 M (near the coast) – 5 M Cl⁻ (rock salt) and a considerable concentration of Br⁻. [20–23] Chloride and bromide can significantly affect the G-values (mole / J, the number of moles produced or consumed per joule of absorbed radiation energy) of water radiolysis products, [24–28] and thereby influence the oxidative dissolution of UO₂ under exposure to ionizing radiation condition. Generally, the complexes formed between halides and UO₂²⁺ are considered to be weak. [12,8] Metz et al. [29] studied radiation induced corrosion of UO₂ pellets at elevated hydrogen pressure in 6 mol (kg H₂O)⁻¹ NaCl solution with and without traces of added bromide. The authors concluded that the uranium (U) on the pellet surface was

* Corresponding author.

E-mail address: ljunyi@kth.se (J. Li).<https://doi.org/10.1016/j.apsusc.2023.158955>

Received 30 June 2023; Received in revised form 14 November 2023; Accepted 17 November 2023

Available online 19 November 2023

0169-4332/© 2023 The Authors. Published by Elsevier B.V. This is an open access article under the CC BY license (<http://creativecommons.org/licenses/by/4.0/>).

significantly oxidized with the formation of clarkeite or meta-schoepite as secondary phases based on a variety of spectroscopy measurements. The authors also recommended further research investigating the influence of bromide and chloride on radiation induced corrosion of UO_2 in less concentrated aqueous solutions. In this work, we have experimentally studied the dissolution behavior of UO_2 exposed to γ - radiation in pure water and in 1 M aqueous solutions of either Cl^- or Br^- . The results are discussed in view of surface reactions. UO_2 pellets after exposures to γ - radiation in these solutions were characterized using X-ray Photoelectron Spectroscopy (XPS) and Ultraviolet Photoelectron Spectroscopy (UPS) to study the oxidation states of U and potential surface alteration.

2. Experimental section

H_2O_2 30 % (Merck), NaHCO_3 (Merck), Br_2 (Merck), Arsenazo III (Sigma-Aldrich), KI (Merck) and $\text{C}_6\text{H}_8\text{O}_6$ (Merck) with Milli-Q water (18.2 M Ω cm) were used to prepare stock solutions. Reagent grade chemicals were used unless otherwise stated. UO_2 pellets were supplied by Westinghouse AB (352 mm² geometrical surface area). [30] UO_2 powder was supplied by Westinghouse Electric Sweden AB. The specific surface area and the mean particle size (diameter) for the UO_2 powder were previously determined as 4.6 ± 0.2 m²/g and 20.2 μm , respectively. [31] The pH of the leaching solutions was measured immediately after the leaching experiment using a pH meter (Orion 4 star, Thermo Scientific) with a glass (ion selective) electrode. There are no acids, bases or buffers used to control the pH of the leaching solutions. The pH meter was calibrated by measuring commercial (Thermo Scientific) pH buffers with 4.01, 7.00, 10.01 pH values.

2.1. Quantitative analysis of H_2O_2 , UO_2^{2+} and Br_3^-

The concentration of H_2O_2 was measured using the Ghormley triiodide method, where I^- was first oxidized to I_3^- by H_2O_2 , and then the absorbance of I_3^- was measured at $\lambda = 360$ nm by a UV/vis spectrophotometer (Thermo Scientific Genesys 20 spectrophotometer). For the H_2O_2 measurement, 1.8 mL of diluted sample was mixed with 100 μL of 1 M KI and 100 μL of 1 M $\text{CH}_3\text{COOH}/\text{CH}_3\text{COO}^-$ buffer containing molybdate as a catalyst in a quartz cuvette.

The concentration of UO_2^{2+} in aqueous phase was spectrophotometrically measured by the Arsenazo III method. Arsenazo III is a dye, which interacts with UO_2^{2+} and forms a stable complex with maximum absorbance at $\lambda = 653$ in acid media. A Thermo Scientific Genesys 20 spectrophotometer was used to measure the absorbance. For the UO_2^{2+} measurement, 0.4 mL sample was diluted to 1.5 mL using Milli-Q water and then mixed with 40 μL of 16 wt% Arsenazo-III reagent and 60 μL of 1 M HCl.

UV-vis spectrophotometry was used to distinguish Br_3^- and H_2O_2 , since Br_3^- has a sharp and intensive peak at 267 nm. Note that Br_3^- can oxidize the Arsenazo III reagent in UO_2^{2+} measurement. For this reason, Ascorbic acid was used as a mild reducing agent to protect the Arsenazo III reagent from oxidation. For the measurement of UO_2^{2+} involving Br_3^- , 0.4 mL sample was diluted to 1.36 mL with pure water and mixed with 1 M HCl (60 μL), 16 wt% Arsenazo-III reagent (40 μL) and 40 mM Ascorbic acid (40 μL) in a cuvette. The detection limits are 0.51 μM , 0.22 μM and 0.30 μM for H_2O_2 , UO_2^{2+} and Br_3^- respectively.

2.2. Pre-washing of UO_2 pellets and UO_2 powder

Before dissolution experiments, each UO_2 pellet was washed in de-aerated 10 mM HCO_3^- to remove the pre-oxidized phase, as UO_2^{2+} can form highly soluble complexes with $\text{HCO}_3^-/\text{CO}_3^{2-}$. Each washing step took 24 h with 3 changes of the 10 mM HCO_3^- solution. The washing process are given in the [supporting information](#) in detail. The washing process for UO_2 powder is also shown in [supporting information](#).

2.3. Dissolution of UO_2 exposed to γ - Radiation in various solutions

Washed UO_2 pellets were submerged in 40 mL of pure water and 1 M aqueous solutions of either Cl^- or Br^- respectively. The pellets were placed on glass pearls to maximize the surface area exposed to the solution. Irradiations were emitted by a Cs-137 gamma source (0.11 Gy s⁻¹ dose rate determined by Fricke dosimetry). The Fricke dosimeter solution was prepared using 1 mM $\text{Fe}(\text{NH}_4)_2(\text{SO}_4)_2$, 1 mM NaCl and 400 mM H_2SO_4 . Upon radiolysis of the aqueous Fricke solution, the oxidizing aqueous radiolysis products oxidize Fe^{2+} to Fe^{3+} . This in turn induces a change in absorbance. The absorbance of the Fricke solution was measured at 304 nm by UV-Vis with the molar absorptivity (ϵ) of 2174 cm⁻¹ M⁻¹ for Fe^{3+} .⁶

γ -radiation exposures were performed at ambient temperature. Prior to the exposures, the solutions were purged with N_2 for 20 min and then sealed tightly with septa and parafilm. There were three UO_2 pellets used in the leaching experiments. UP-1 (UO_2 pellet #1) was first exposed to γ - radiation in pure water followed by in 1 M Cl^- solution and finally in 1 M Br^- solution, UP-2 (UO_2 pellet #2) was first exposed to γ - radiation in 1 M Cl^- solution followed by in 1 M Br^- solution and finally in pure water, and UP-3 (UO_2 pellet #3) was first exposed to γ - radiation in 1 M Br^- solution followed by in pure water and finally in 1 M Cl^- solution. UO_2^{2+} concentration was measured as a function of irradiation time. 1.5 mL aliquots were taken from the solution for each measurement. Syringe and needle were used to take aliquots through the rubber septum to avoid exposure to the atmosphere. Between the exposures, the UO_2 pellets were washed according to the washing procedures mentioned before.

2.4. Br_3^- induced dissolution of UO_2 powder

25, 50, 75 and 100 mg of UO_2 powders were added to 25 mL of aqueous solutions containing 0.2 mM Br_3^- , respectively. The samples were stirred to a homogeneous suspension throughout the experiment and purged with N_2 . The surface area to solution volume ratio (S/V) for the suspensions are 4.6×10^3 m⁻¹, 9.2×10^3 m⁻¹, 13.8×10^3 m⁻¹ and 18.4×10^3 m⁻¹, respectively. For each sampling, 1–2 mL suspension was taken using a syringe followed by immediate filtering the suspension with a 0.2 μm cellulose acetate syringe filter.

2.5. XPS and UPS

The photon energy used in the XPS and UPS measurements is 1486.6 eV (monochromatized Al K α source) and 40.8 eV (standard He-discharge lamp He II source), respectively. The electron analyzer is a Scienta ESCA 200 hemispherical spectrometer. The spectra were collected in an ultrahigh vacuum surface analysis system with a base pressure of 5×10^{-10} mbar. The XPS binding energy was calibrated by the Fermi edge at 0 eV and the Au 4f_{7/2} line at 84.0 eV for valence band spectra and core level spectra, respectively. The UPS binding energy was calibrated with the Fermi edge at 0 eV. The total energy resolution of XPS was set such that the FWHM (full width at half-maximum) of the clean Au 4f_{7/2} line (at the binding energy of 84.00 eV) to be 0.65 eV. The resolution of the UPS measurements was approximately 0.1 eV (estimated from the Fermi edge of clean gold). [32] XPS and UPS spectra were recorded at ambient temperature and normal emission. The form of the samples is solid UO_2 slices (0.15 mm thickness). Prior to photoelectron measurements, the samples were rinsed with Milli-Q water and dried in a glove box ($\text{O}_2 \leq 0.1$ ppm). Note that this (second) washing step has a different purpose from the first washing step mentioned above, the second washing step is to remove any soluble species on the UO_2 surface after exposures. The samples were transported to the photoelectron spectrometer using Ar-filled Polypropylene tubes. The measured samples had good conductivity, and there is no analyzer effect on the samples (no charge problem nor beam damage).

The software used for XPS and UPS data analysis is Thermo Avantage

Software© (ver. 5.9931). Shirley background subtraction was used throughout the spectra fitting with an additional constraint i.e., at any range, the background intensity was not allowed to exceed the raw data intensity. The raw data was smoothed using Savitzky – Golay filtering (1 eV window size and 4 polynomial). A fixed 20 % Gaussian – Lorentzian characteristic was used in peak deconvolution unless otherwise stated. Specific principles and parameters for U 4f, O 1 s, O 2p and U 5f peak deconvolution were described in detail in the corresponding results part with reference support. Satellite peaks generated by U 4f main peaks were separated and discussed in detail. Errors in fitting parameters can be seen from the discrepancy between the cumulative fit and raw data.

3. Results and discussion

Irradiation of pure water and 1 M aqueous solutions of either Cl^- or Br^- without UO_2 pellets was first performed to investigate the evolution of H_2O_2 in these aqueous systems. The results are shown in Fig. 1. The experiments were repeated four times. As can be seen, in all the aqueous solutions, the H_2O_2 concentration increases until it reaches steady-state. The steady-state concentration of H_2O_2 in pure water under the present irradiation conditions is approximately 0.15 mM. Joseph et al. [33] studied H_2O_2 concentrations in either argon- or air-saturated ultra-pure water (no other solutes) with no headspace at a dose rate of 2.5 Gy / s. Experimental results shown that the H_2O_2 concentrations are 0.9 mM in aerated water and lower than detection limit (3 μM) in deaerated water. The steady state H_2O_2 concentration in 1 M Cl^- solution is 0.03 mM, which is 5 times lower than that in H_2O . The lower steady-state H_2O_2 concentration in Cl^- solution exposed to γ -radiation compared to in H_2O has also been reported by Hata et al. [34]. Interestingly, the steady state concentration of H_2O_2 in this work appears to be highest in the 1 M Br^- solution. However, it is noteworthy that in irradiated solutions containing Br^- , Br_3^- can also be formed. [35–37].

Br_3^- is an oxidant thermodynamically capable of oxidizing I^- to I_3^- . [38] Consequently, the measured I_3^- absorbance in the Ghormley triiodide method for H_2O_2 detection can be attributed to both H_2O_2 and Br_3^- . To check the influence of the absorbance of H_2O_2 (and UO_2^{2+}) on the absorbance of Br_3^- , spectra of Br_3^- , H_2O_2 and UO_2^{2+} at 0.03 mM and the spectrum of a solution containing equimolar mixture of Br_3^- , H_2O_2 and

UO_2^{2+} at 0.03 mM were recorded (Fig. 2). Br_3^- was synthesized by adding Br_2 to a solution containing excess concentrations of Br^- (reaction 1), with the equilibrium constant $K = 17 \text{ L/mol}$. [39,36].



As can be seen in Fig. 2, the absorbances of UO_2^{2+} and H_2O_2 are negligible at 267 nm wavelength. [36,39]. The calibration curve to determine the Br_3^- concentration from absorbance is shown in figure S1.

3.1. Dissolution of UO_2 in pure water and 1 M aqueous solutions of either Cl^- or Br^- exposed to γ – radiation

Fig. 3 shows the UO_2^{2+} release from a UO_2 pellet (UP-1) in pure water and 1 M aqueous solutions of either Cl^- or Br^- exposed to γ – radiation. The dissolution experiments were performed using three UO_2 pellets (UP-1, UP-2 and UP-3). Since the results of dissolution experiments for UP-2 and UP-3 are generally similar to UP-1 and different UO_2 pellets can display different redox reactivity, the results for UP-2 and UP-3 were plotted separately. These plots can be found in the supporting information (figure S2 and S3). There was no noticeable difference in the results for the different pellets under comparable conditions. Hence, the results are independent of the order of the different exposures. Concentrations corrected for changes in solution volume were used in this work, because sampling will result in decreased solution volume with time. Normalization details are given in the supporting information.

As can be seen in Fig. 3, the H_2O_2 concentration first increases and then remains at about 0.15 mM (steady state) in pure water, while the concentration of UO_2^{2+} first increases to 0.025 mM and then decrease as a function of time. Both the H_2O_2 and UO_2^{2+} concentrations were measured in doublets, and the uncertainty between the two measurements is less than 4.5 μM and 0.9 μM , respectively. The decrease in UO_2^{2+} concentration probably indicates the formation of uranyl peroxide (studtite $\text{UO}_2\text{O}_2 \cdot 4\text{H}_2\text{O}$) through the reaction between dissolved UO_2^{2+} and H_2O_2 . The H_2O_2 concentration in 1 M Cl^- solution increased more slowly than in pure water, and then remained at the steady-state concentration (0.04 mM). However, there was almost no detectable UO_2^{2+} in the solution. Interestingly, in 1 M Br^- solution, the UV–Vis spectrophotometer detected a sharp peak at 267 nm indicating the presence of Br_3^- . By using the measured absorbance and the calibration curve in figure S1, the concentration of Br_3^- was calculated. As shown in Fig. 3, the dominant species during the first 20 h in 1 M Br^- solution exposed to γ –

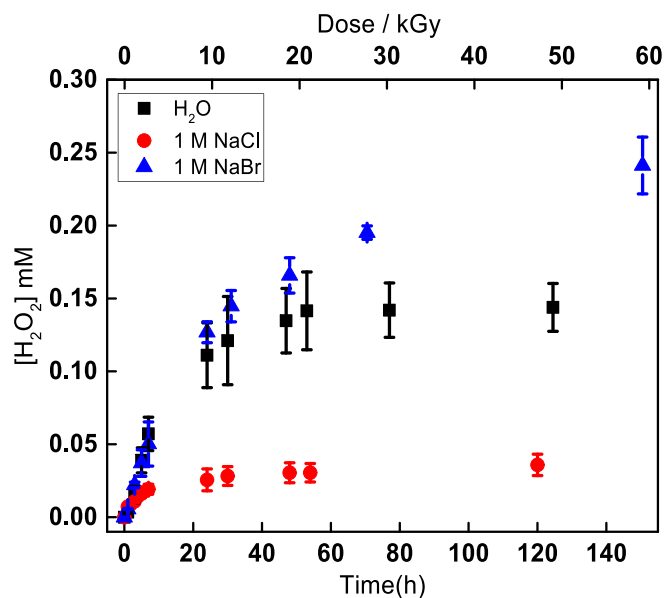


Fig. 1. Concentration of H_2O_2 as a function of time (bottom axis) and dose (top axis) in solutions containing H_2O (black), 1 M Cl^- (red) and 1 M Br^- (blue) exposed to γ -radiation. (For interpretation of the references to colour in this figure legend, the reader is referred to the web version of this article.)

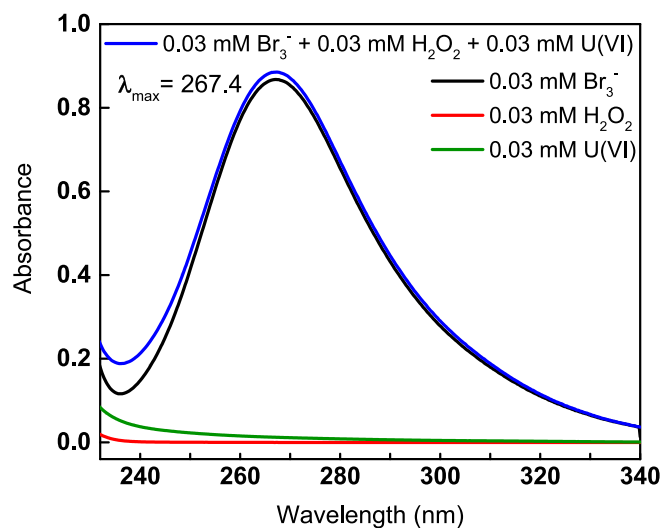


Fig. 2. UV–vis spectra of solutions containing 0.03 mM Br_3^- (black), 0.03 mM H_2O_2 (red), 0.03 mM UO_2^{2+} (green) and 0.03 mM Br_3^- , 0.03 mM H_2O_2 , 0.03 mM UO_2^{2+} (blue). (For interpretation of the references to colour in this figure legend, the reader is referred to the web version of this article.)

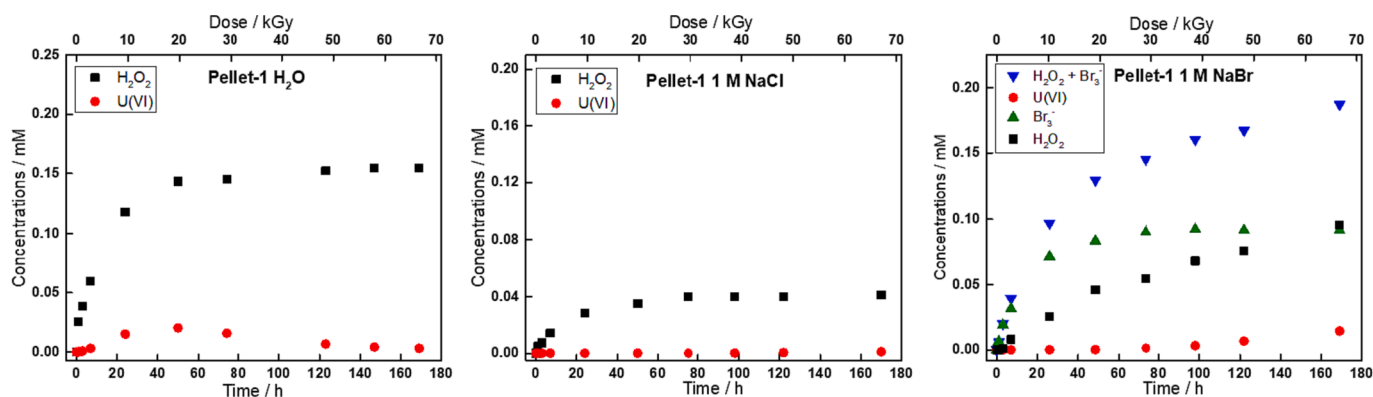


Fig. 3. Concentrations of H_2O_2 (black square), UO_2^{2+} (red circle) and Br_3^- (green triangle) as a function of time (bottom axis) and dose (top axis) in solutions containing the UO_2 pellet-1 with H_2O , 1 M Cl^- and 1 M Br^- . The pH was 6.19, 5.87 and 8.86 (measured at the end of the experiment for Cl^- and Br^- systems, respectively). (For interpretation of the references to colour in this figure legend, the reader is referred to the web version of this article.)

radiation is Br_3^- . After 24 h, the concentration of Br_3^- remains stable and the H_2O_2 concentration gradually increases. The dissolved UO_2^{2+} concentration is virtually 0 during the first 40 h, followed by a slight increase along with the increase in H_2O_2 concentration. XPS results (shown below) show that the UO_2 surface was oxidized to UO_{2+x} without the formation of any other secondary phases after exposure to γ - radiation in saline solutions. This indicates that the U(IV)O_2 was first oxidized to U(V) and U(VI) , with the U(V) accumulated on the surface, and U(VI) adsorbed and desorbed on the UO_2 surface. The UO_2^{2+} adsorption effect is a surface phenomenon induced by ionic strength. [40] Previous work has shown that the externally added UO_2^{2+} or UO_2^{2+} formed from oxidative dissolution can rapidly be adsorbed on UO_2 surface in 1 M aqueous solutions of either Cl^- or Br^- . [40].

To check the redox reactivity of UO_2 exposed to Br_3^- , experiments using synthesized Br_3^- and UO_2 powder were performed. The results of 0.2 mM Br_3^- induced dissolution of 50 mg and 100 mg UO_2 powder are shown in Fig. 4, while the results for 25 mg and 75 mg UO_2 powder are shown in figure S4 (similar trend). The 1st-order rate constants were plotted as a function of the surface to volume ratio to determine the second order rate constant. A linear regression based on $\ln[\text{Br}_3^-]$ versus time was used to calculate the 1st-order rate constants, and the time interval used in the linear regression is from 0 to 110 min (the last measurement time point was not included). In general, the concentration of dissolved UO_2^{2+} increased quantitatively as the concentration of Br_3^- decreased demonstrating the oxidative capability of Br_3^- towards UO_2 .

3.2. Adsorption of UO_2^{2+} on UO_2 surface in the leaching solutions

Unlike the irradiated pellet in 1 M aqueous solution of Br^- , oxidation of the UO_2 powder by Br_3^- leads to dissolution of UO_2^{2+} . The reason why

the irradiated pellet does not dissolve like the powder does can be explained by the pH of the system and the point of zero charge of UO_2 . Since in 1 M aqueous solutions of either Cl^- or Br^- under γ - radiation exposure condition (shown in Fig. 3), the pH were 5.87 and 8.86 (measured at the end of the experiment for Cl^- and Br^- systems respectively), which were all higher than the point of zero charge of UO_2 (5.8) [41,42]. Hence the surface will be negatively charged and favor the UO_2^{2+} adsorption. In Br_3^- induced dissolution of UO_2 experiment (shown in Fig. 4), the pH of the 0.2 mM Br_3^- in 1 M Br^- is 3.91 (measured at the beginning of the experiment), and the dissolved UO_2^{2+} can decrease the pH further due to the hydrolysis of UO_2^{2+} . As a result, the pH of the system is lower than the point of zero charge of UO_2 resulting in a positively charged UO_2 surface, which in turn counteracts the UO_2^{2+} adsorption.

In addition, the gradually increasing of the concentration of UO_2^{2+} in the 1 M Br^- solution (shown in Fig. 3) after 40 h can be attributed to two possible reasons. The first possibility is the speciation change of UO_2^{2+} . By using the same speciation calculation method reported in our previous paper, [12] it was found that due to the increase of concentration of H_2O_2 with experimental time, speciation of UO_2^{2+} changed from UO_2^{2+} , UO_2Br^+ and UO_2OH^+ to $(\text{UO}_2)(\text{O}_2)(\text{Br})(\text{H}_2\text{O})_2$ (Figure S9 and S10). $(\text{UO}_2)(\text{O}_2)(\text{Br})(\text{H}_2\text{O})_2$ complex is the dominating species at the end of the monitoring of the leaching experiment in 1 M aqueous solution of Br^- . The negatively charged complex $(\text{UO}_2)(\text{O}_2)(\text{Br})(\text{H}_2\text{O})_2$ will be electrostatically repelled by the negatively charged surface, and be detected from the bulk leaching solution. Previous control experiments have shown that speciation does not affect the results of the methods used to determine the total concentrations of uranium. [43] The second possibility is that the UO_2^{2+} adsorption capacity on UO_2 is limited. As the observed oxidant concentration is higher in 1 M Br^- as compared to 1 M

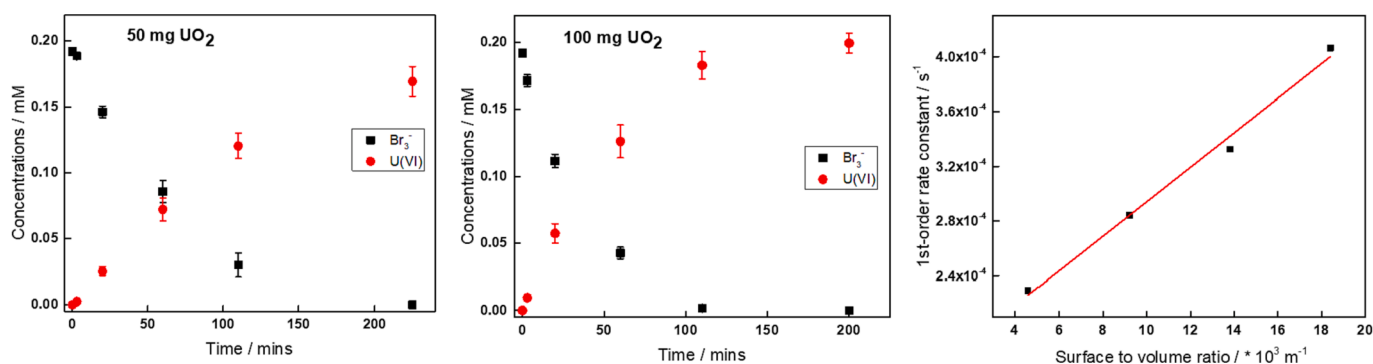


Fig. 4. Concentrations of Br_3^- (black square) and UO_2^{2+} (red circle) as a function of time in aqueous 50 mg and 100 mg UO_2 powder suspensions containing 0.2 mM Br_3^- and 1 M Br^- . (For interpretation of the references to colour in this figure legend, the reader is referred to the web version of this article.)

Cl⁻, it is possible that UO_2^{2+} surface saturation is reached in the former case.

The water radiolysis products such as HO•, HO₂•, and H₂O₂ mainly contribute to the oxidation of UO_2 under irradiation. In addition, the peroxide group formed by water radiolysis can contribute to the stabilization of the dissolved UO_2^{2+} in the bulk 1 M aqueous solution of Br⁻ by forming uranyl-peroxo-bromo ternary complexes. [12].

3.3. Surface characterization

3.3.1. XPS

The UO_2 pellets after exposures to pure water and 1 M aqueous solutions of either Cl⁻ or Br⁻, respectively, were characterized by XPS with one reference sample measured after the washing step representing the starting point of the samples. Full XPS scans of reference sample and samples after exposures to γ -radiation in pure water and 1 M aqueous solutions of either Cl⁻ or Br⁻ were performed, and the spectra show that the only elements present on the surface are U, O and C (Figure S5-S8).

Four methods were used to determine the oxidation states of the U from XPS spectra in this work: (1) deconvolution analysis of the U 4f_{7/2} main peak; (2) the energy difference between the U 4f_{5/2} main peak and the satellite peaks; (3) peak shape (FWHM and peak centers) of the O 1s peaks; (4) comparison of the U 5f to O 2p_{3/2} peak area ratio. [44–48] Note that quantitative analysis was only applied for method 1.

Fig. 5 shows the XPS narrow U 4f scans. The measured U 4f_{5/2} and U 4f_{7/2} main peaks in the reference sample are close to 390.8 and 380.0 eV. The peak positions are in line with references reported U 4f_{7/2} and U 4f_{5/2} peaks of UO_2 . [44,45,47] Both U 4f_{7/2} and U 4f_{5/2} peaks shift to higher binding energy after exposure to γ -radiation in the three solutions (H₂O, 1 M Cl⁻, 1 M Br⁻) showing that the surfaces were oxidized and the average oxidation state of U increased. The U 4f peaks from the sample in pure water exposed to γ -radiation shifts further compared to the samples in saline solutions indicating a higher average oxidation state of U.

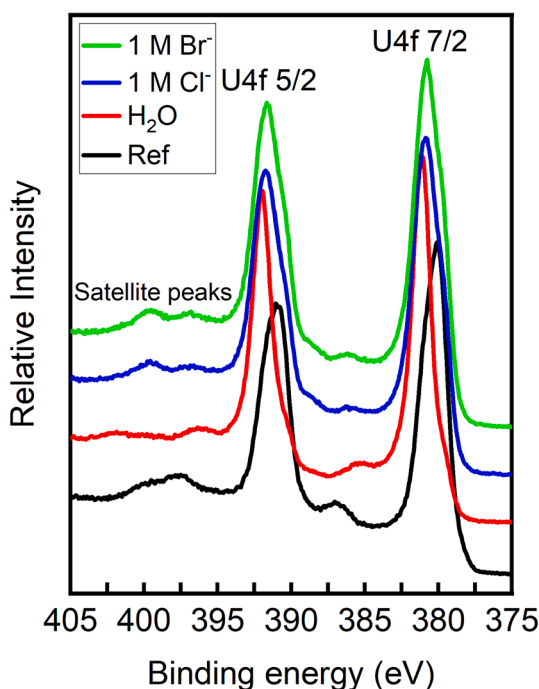


Fig. 5. U 4f spectra of UO_2 surfaces after exposure to γ -radiation in pure water and in 1 M aqueous solutions of either Cl⁻ or Br⁻ plotted together with a reference sample.

3.4. U 4f spectra analysis and deconvolution principle

The stoichiometric ratio of U/O (degree of oxidation) can be studied quantitatively by deconvolution of the U 4f_{7/2} peak into the component U (IV), U(V) and U(VI) peaks. [47–49] Note that the U 4f_{5/2} peak is not suitable for deconvolution because the satellite peaks of the U 4f_{7/2} peak can influence the shape of the U 4f_{5/2} peak. The deconvolution principle is essential for quantitative analysis and the deconvolution principle for the U 4f_{7/2} peak used in this work is the same as the principle used in our previous work. [32] Briefly, a 20 % Gaussian-Lorentzian characteristic, a fixed 1.40 eV of FWHM for deconvoluted U(VI), U(V) and U(IV) peaks were used. The peak centers of the deconvoluted peaks were allowed to vary slightly around the reported values for pure materials with a controlled distance of 1.0 eV between the U(IV) and the U(V) peaks. [49–52].

Fig. 6 shows the deconvolution of U 4f_{7/2} peaks (U(IV) in red, U(V) in blue and U(VI) in cyan). Note that no clear U(VI) peak (~382 eV) can be identified during the deconvolution (software, Avantage, ver. 5.9931) in the reference sample and oxidized UO_2 in 1 M Cl⁻ / Br⁻ solutions. The reason for the absence of detectable U(VI) is due to the rinsing with water prior to XPS analysis. The highly soluble U(VI) - Br⁻/Cl⁻ complexes are weak in terms of the affinity of Br⁻/Cl⁻ to U(VI). The complexes are weak but that the very high halide concentrations drive the equilibrium towards the complexes and thereby enhances the U(VI) solubility. Interestingly, a U(VI) peak can be clearly identified for the pellet in H₂O exposed to γ -radiation. This indicates that either the UO_2 was oxidized to UO_3 , or a secondary uranyl phase was formed on UO_2 surface. Since the FWHM of uranyl peroxide is larger than that for uranium oxides, and the multiple splitting phenomenon on the FWHM of U(VI), U(V) and U(IV) peaks in mixed uranyl peroxide and oxidized uranium dioxide system is not clear. The FWHM of U(VI), U(V) and U(IV) was allowed to vary, but FWHM of U(IV) and U(V) peaks was kept identical during deconvolution. [50,52] Deconvolution results show that the U(VI) peak matches well the meta-studtite ($\text{UO}_2\text{O}_2 \cdot 2\text{H}_2\text{O}$) peak reported in ref [53] (381.9 ± 0.2 eV; FWHM = 1.8 eV). In addition, the peak area of U(V) is larger in the UO_2 samples exposed to γ -radiation in pure water and in 1 M aqueous solutions of either Cl⁻ or Br⁻ compared to the unexposed reference sample. U(VI) was only observed on the surface after exposure to γ -radiation in pure water, and the U(VI) was assigned to the secondary phase $\text{UO}_2\text{O}_2 \cdot 2\text{H}_2\text{O}$ (not UO_3). For the other exposures, the area ratio between the U(V) and U(IV) peaks was used to determine the stoichiometric ratio of U/O of the hyper-stoichiometric UO_2 (mole fraction of U (IV), U(V) and U(VI) was shown in Table S1). The percentage of the formed meta-studtite on the oxidized UO_2 surface was also calculated. The calculated results and the summary of deconvolution are shown in Table 1.

The oxidation states of U can also be seen from the peak positions of the satellite peaks of U 4f_{5/2} and the energy difference between U 4f_{5/2} main peak and the satellite peaks. The peak positions and the energy difference mentioned above are summarized in Table 2. In the reference sample (shown in Fig. 5), the energy difference between U 4f_{5/2} main peak and the satellite peak is 6.7 eV, which is in line with the value for a pure U(IV) material (6.9 ± 0.2 eV). [47] Interestingly, an inconspicuous satellite peak 8.45 eV from the main peak indicates that the reference sample also contains some U(V). Two satellite peaks can be observed for the samples in both 1 M Cl⁻ and 1 M Br⁻ solutions, with the energy differences of approximately 5.1 eV and 7.8 eV, respectively. The satellite peak located 7.8 eV from the main peak of U(V) is more intense than the satellite peak located 5.1 eV from the main peak of U(IV), implying that U(V) is the dominating oxidation state. [44] The similar peak positions of U 4f_{5/2} satellite peaks between the Cl⁻ and Br⁻ systems also indicate a close final stoichiometric ratio of U/O in the uranium oxides exposed to the two systems. In addition, the sample in pure water shows two satellite peaks with the energy differences of 4.4 and 9.9 eV respectively, close to the reference reported 4.4 and 9.7 eV for U(VI). [44] However, the satellite peak with 9.9 eV shift is quite board due to the overlap with

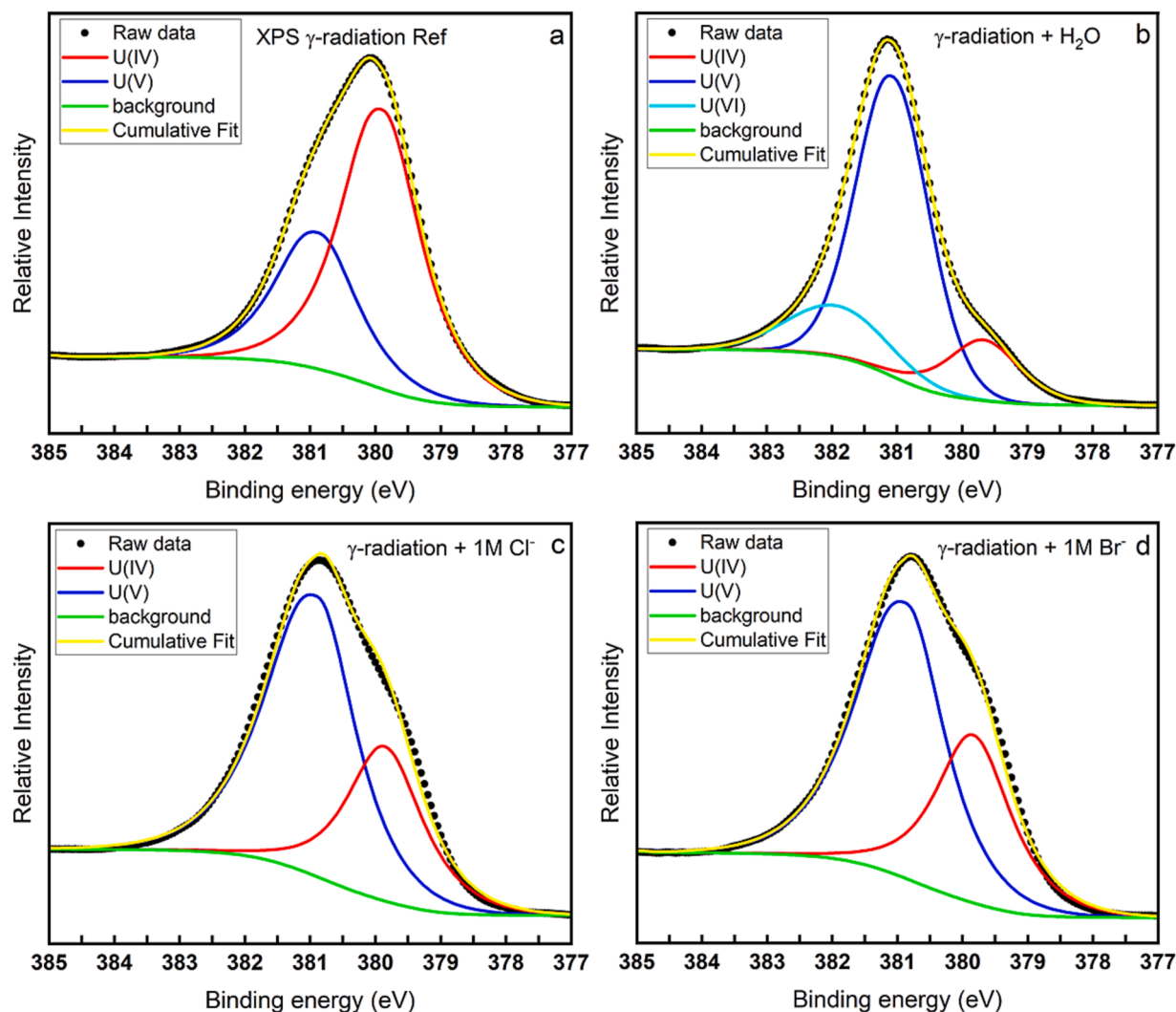


Fig. 6. Deconvolution of U $4f_{7/2}$ into U (IV) $4f_{7/2}$, U (V) $4f_{7/2}$ and U (VI) $4f_{7/2}$.

Table 1

Summary of peak positions, FWHM, calculated stoichiometry and percent of U in meta-studtite of the deconvoluted peaks from U $4f_{7/2}$ peaks.

| Solutes | peak position of U (IV) | Peak position of U (V) | Peak position of U (VI) | FWHM of U (IV) | FWHM of U (V) | FWHM of U (VI) | Calculated stoichiometry | Percent of U in meta-studtite |
|---------------------|-------------------------|------------------------|-------------------------|----------------|---------------|----------------|--------------------------|-------------------------------|
| Ref | 379.89 | 380.87 | – | 1.40 | 1.40 | – | UO _{2.17} | – |
| None | 379.67 | 381.07 | 381.92 | 1.35 | 1.35 | 1.82 | UO _{2.41} | 16.1 % |
| 1 M Cl ⁻ | 379.86 | 380.88 | – | 1.40 | 1.40 | – | UO _{2.34} | – |
| 1 M Br ⁻ | 379.84 | 380.86 | – | 1.40 | 1.40 | – | UO _{2.33} | – |

Table 2

Summary of the U $4f_{5/2}$ peak positions and the energy difference between the U $4f_{5/2}$ main peak and satellite peaks.

| Solutes | U $4f_{5/2}$ peak position (eV) | Satellite peak (S1) position (eV) | Satellite peak (S2) position (eV) | Distance between U $4f_{5/2}$ and S1 (eV) | Distance between U $4f_{5/2}$ and S2 (eV) |
|---------------------|---------------------------------|-----------------------------------|-----------------------------------|---|---|
| Ref | 391.05 | 397.5 | 399.5 | 6.65 | 8.45 |
| None | 391.95 | 396.35 | 401.85 | 4.4 | 9.9 |
| 1 M Cl ⁻ | 391.8 | 396.85 | 399.6 | 5.05 | 7.8 |
| 1 M Br ⁻ | 391.65 | 396.8 | 399.5 | 5.15 | 7.85 |

the satellite peak generated from U(V).

3.5. O 1s spectra analysis

Fig. 7 shows the O 1s spectra. In the reference sample, three component peaks can be obtained from the deconvolution. These component peaks are located at 530.1, 531.3 and 532.9 eV, with the FWHM of 1.22, 1.20 and 1.20 eV, respectively. The Peak at 530.1 eV is assigned to the O in hyper-stoichiometric UO_{2+x} and the peaks at 531.3 eV and 532.9 eV are assigned to OH⁻ and CO₃²⁻ respectively. [45] The CO₃²⁻ peak was only observed for the reference sample since it was stored in 10 mM HCO₃⁻ during the same experimental time. After UO₂ was exposed to γ -radiation in 1 M aqueous solutions of either Cl⁻ or Br⁻, the O 1s peaks of oxidized UO₂ and OH⁻ move to lower binding energies (529.8 eV and 531.0 \pm 0.1 eV, respectively) indicating that there is a

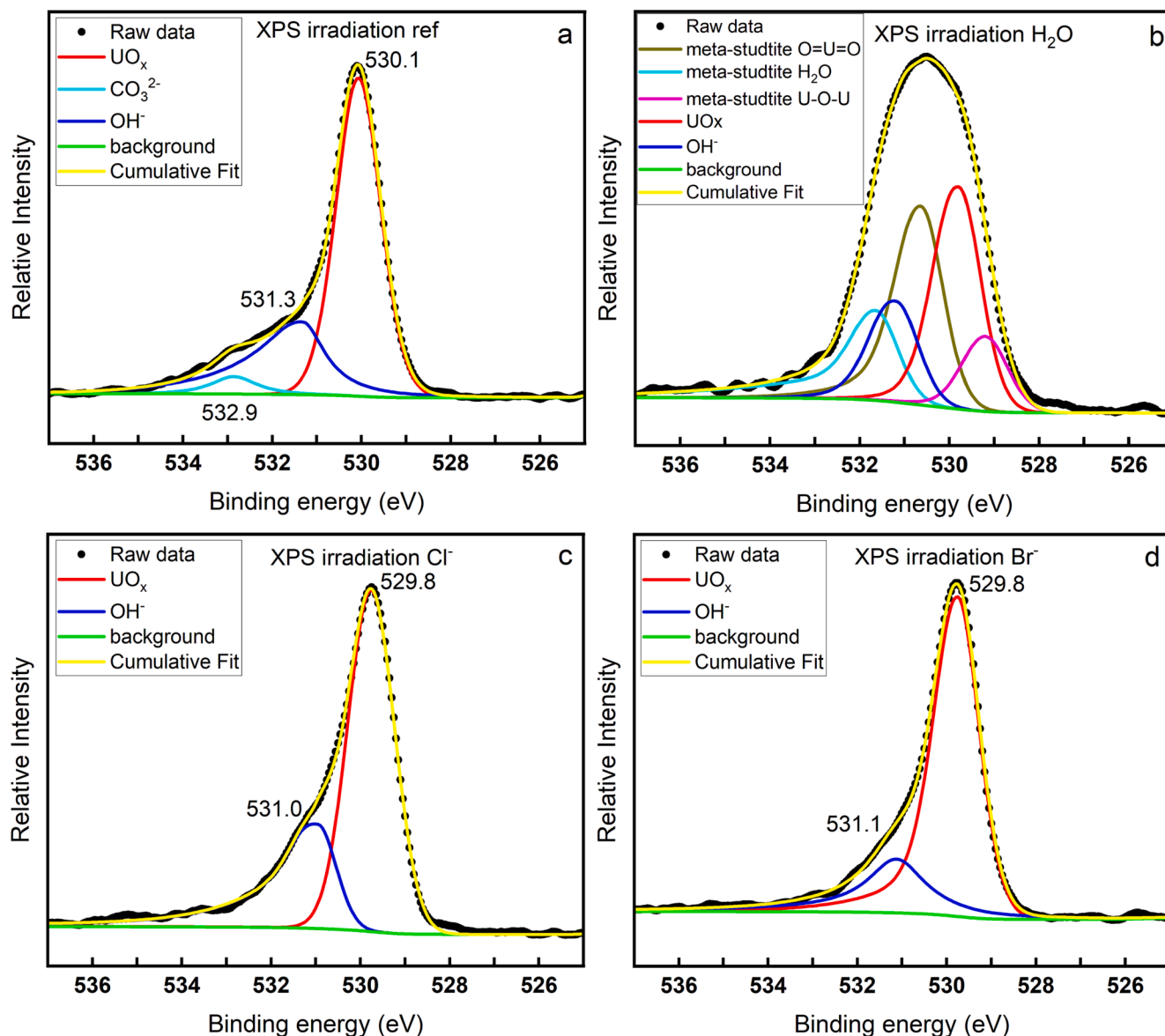


Fig. 7. O 1s spectra of the reference sample and UO_2 surfaces after exposure to γ -radiation in pure water and in 1 M aqueous solutions of either Cl^- or Br^- with their deconvolution feature.

change of the chemical environment of O after exposure. The absence of a difference in O 1s peak position of the samples exposed to γ -radiation in 1 M Cl^- and 1 M Br^- shows that the final stoichiometric ratio of U/O is the same under these conditions. Interestingly, the sample in pure water exposed to γ -radiation shows a much broader peak compared to other samples. The broadness of the peak from 528 eV to 534 eV indicates that the sample contains a secondary phase on oxidized UO_2 , and the peak broadness from 528 eV to 534 eV is in line with the reported values for meta-studtite. [53,54] The deconvolution of this peak was performed according to the O in meta-studtite in ref [54] and O in oxidized UO_2 in this work with the FWHM of all the component peaks fixed at 1.20 eV. The structure of meta-studtite comprises of infinite chains of uranyl peroxides with repeated hexagonal bipyramids. There are 3 different groups containing O including UO_2^{2+} , O-U-O, H_2O (directly connected to UO_2^{2+}). As can be seen in Fig. 7b, the O1s peak fitting matches the raw data well confirming the co-existence of meta-studtite and oxidized UO_2 . As drying studtite in O_2 and H_2O deficient environment will result in irreversible transformation from studtite to meta-studtite, [10,55] and we dried the sample in glove box after rinsing, we cannot conclude whether studtite or meta-studtite was formed on the original sample. It

is most probable that the originally formed secondary phase was studtite, since formation of meta-studtite in aqueous solutions generally requires temperature higher than 70 °C. [10] In addition, there is no indication of O peaks of meta-studtite in the O 1s spectra of the samples in halide solutions exposed to γ -radiation. This is in line with previously reported that high ionic strength (1 M) can significantly inhibit the studtite formation. [12].

3.6. XPS and UPS U 5f spectra analysis

Figs. 8 and 9 show the measured XPS and UPS U 5f spectra (valence band region). UPS is a more surface sensitive tool that has an information depth of 1 monolayer compared to XPS that has an information depth of 5 monolayers. In Figs. 8 and 9, the peaks at approximately 1.4 eV represent the U 5f peaks. While the peaks at the range of 2.5 eV – 12.5 eV are a combination of O $2p_{3/2}$ peaks and O $2p_{1/2}$ peaks. The binding energy of the O $2p_{3/2}$ peak is lower than that of O $2p_{1/2}$ peak. U (VI), U(V) and U(IV) have the $[\text{Rn}]5f$, $[\text{Rn}]5f^1$, $[\text{Rn}]5f^2$ electronic configuration, respectively. The U 5f peak area is directly related to electron population in the 5f orbital, thus a decrease in U 5f peak area

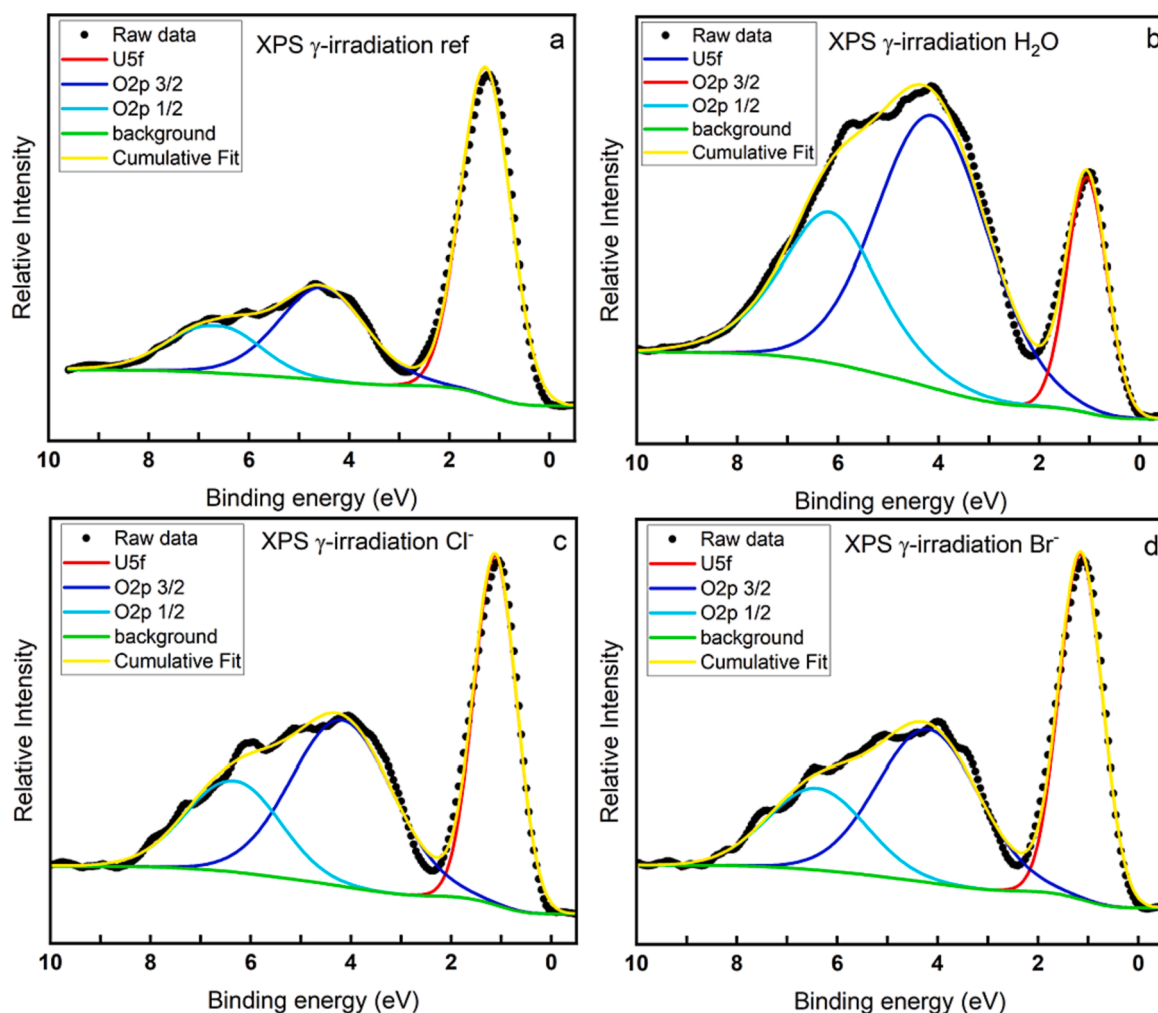


Fig. 8. Valence band spectra (XPS source) of the UO_2 surfaces after exposure to γ -radiation in pure water and in 1 M aqueous solutions of either Cl^- or Br^- with the O 2p peak deconvolution.

can be observed upon U(IV) oxidation. The U 5f peak cannot be observed in U(VI) compounds (no electrons in the 5f orbital). In this work, the U 5f to O $2p_{3/2}$ peak area ratio was used to compare the degree of oxidation of the samples. The deconvolution of the O 2p peak to the component O $2p_{3/2}$ and O $2p_{1/2}$ peaks was performed according to the spin-orbit splitting principle that the O $2p_{1/2}$ peak area should be twice as small as the O $2p_{3/2}$ peak area (2 electrons in the $2p_{1/2}$ level, and 4 electrons in the $2p_{3/2}$ level). The peak broadening (large FWHM) and the imperfect match between raw data and the cumulative fit of the deconvoluted O $2p_{1/2}$ and O $2p_{3/2}$ peaks are attributed to hybridization effects. This has been discussed in a recent publication. [32].

The peak centre, FWHM and the U 5f to O $2p_{3/2}$ peak area ratio in the XPS and UPS spectra are listed in Table 3. It is clear that there is a decrease in the U 5f to O $2p_{3/2}$ peak area ratio for the exposed samples compared to the reference sample (for both UPS and XPS measurements) indicating an increase in the U oxidation state. The narrowing of the U 5f peaks as can be observed from the declined FWHM of the exposed samples is attributed to decreased electron population of in the 5f orbital, which also represents the increased oxidation state. [44] Interestingly, the U 5f peak in the UPS spectra of the sample after γ -radiation exposure in H_2O completely disappear indicating the U on the ultra-thin surface is only in the form of U(VI). In halide systems, the U 5f to O $2p_{3/2}$ peak area ratio in the UPS spectra is significantly smaller than in the corresponding XPS spectra. The extremely small values of the U 5f to O $2p_{3/2}$ peak area ratio in the UPS spectra indicate that the outermost layer of the exposed surfaces most likely consists of U(VI) to a considerable

extent.

3.7. Surface composition at the depth measured by XPS and UPS, respectively

Since XPS and UPS provide information at different depth, the results cannot be directly compared. However, XPS and UPS can provide a rough depth profile. At the depth measured by XPS (10 nm), the sample after exposure to γ -radiation in pure water contains $\text{UO}_{2.41}$ and studtite, while the samples after exposure to γ -radiation in halide solutions contain only $\text{UO}_{2.33}$, (the reason why studtite was not formed is due to the ionic strength effect as mentioned above). At the depth measured by UPS, the sample after exposure to γ -radiation in pure water shows 100 % U(VI), and the samples after exposure to halide solutions show a significant fraction of U(VI). Since the samples were rinsed before XPS and UPS measurements, the U(VI) cannot be originated from adsorbed soluble uranyl species such as uranyl-(peroxo)-halo species. It is not yet understood what is the exact speciation of the U(VI) on the surface at the depth measured by UPS, since the UPS and XPS U 5f spectra analysis is based on a totally different methodology from U 4f and O 1s spectra analysis i.e., informative peak deconvolution cannot be performed. What is clear is that studtite should be formed at the sample surface with UPS detection depth after exposure to γ -radiation in pure water (since studtite was characterized at an even deeper depth measured by XPS). Fig. 10 summaries surface compositions after exposure to γ -radiation in pure water and halide solutions at the depth measured by XPS and UPS,

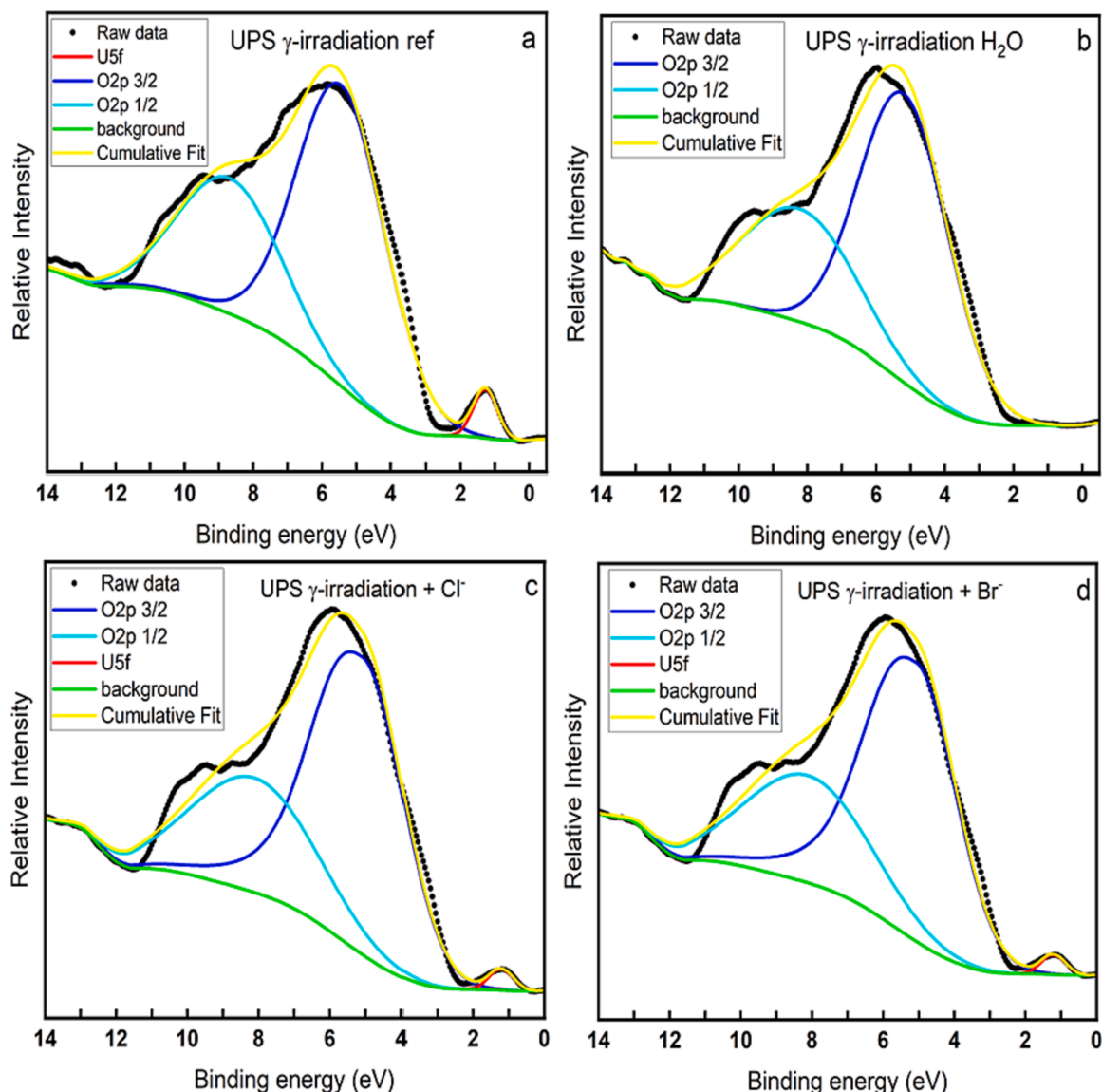


Fig. 9. Valence band spectra (UPS source) of the UO_2 surfaces after exposure to γ -radiation in pure water and in 1 M aqueous solutions of either Cl^- or Br^- with the O 2p peak deconvolution.

Table 3
Summary of peak positions, FWHM, and U 5f to O $2p_{3/2}$ peak area ratio.

| Solutes (Type of photoemission) | peak position of U 5f | Peak position of O $2p_{3/2}$ | FWHM of U 5f | FWHM of O $2p_{3/2}$ | U 5f to O $2p_{3/2}$ peak area ratio of |
|---------------------------------|-----------------------|-------------------------------|--------------|----------------------|---|
| Ref (XPS) | 1.28 | 4.53 | 1.17 | 2.16 | 1.94 |
| None (XPS) | 1.05 | 4.11 | 0.94 | 2.69 | 0.35 |
| 1 M Cl^- (XPS) | 1.12 | 4.17 | 1.01 | 2.46 | 0.88 |
| 1 M Br^- (XPS) | 1.15 | 4.18 | 1.02 | 2.46 | 0.95 |
| Ref (UPS) | 1.27 | 5.44 | 0.82 | 3.05 | 0.043 |
| None (UPS) | – | 5.19 | – | 3.04 | 0 |
| 1 M Cl^- (UPS) | 1.20 | 5.08 | 0.79 | 2.63 | 0.018 |
| 1 M Br^- (UPS) | 1.13 | 5.13 | 0.66 | 2.95 | 0.021 |

respectively.

4. Conclusion

The dissolution of UO_2 exposed to γ -radiation in pure water and 1 M

aqueous solutions of either Cl^- or Br^- was studied. For pure water, the UO_2^{2+} concentration increases significantly during the first 48 h. Thereafter, the UO_2^{2+} concentration decreases. This can be attributed to precipitation of studtite. The low concentration of UO_2^{2+} in 1 M aqueous solutions of either Cl^- or Br^- is attributed to the adsorption of UO_2^{2+} on UO_2 facilitated by the high ionic strength. The adsorption is also affected by the pH of the solution relative to the point of zero charge of UO_2 and the speciation of the UO_2^{2+} . Formation of studtite on oxidized UO_2 surfaces after exposure to γ -radiation in pure water was confirmed by XPS and UPS. In addition, XPS show that the UO_2 surfaces were oxidized with U(V) as the dominating state after exposure to γ -radiation in pure water and 1 M aqueous solutions of either Cl^- or Br^- . The calculated stoichiometric ratios of U/O based on the deconvolution of U $4f_{7/2}$ spectra are 84 % $\text{UO}_{2.41}$ and 16 % (meta)-studtite, $\text{UO}_{2.34}$ and $\text{UO}_{2.33}$, for pure water, 1 M Cl^- and 1 M Br^- solutions, respectively. XPS results show no observable amounts of U(VI) on the oxidized UO_2 surfaces after exposures to γ -radiation in 1 M aqueous solutions of either Cl^- or Br^- , while UPS results confirm the existence of significant amounts of U(VI) on the outer thin layer of oxidized UO_2 after exposures to γ -radiation in 1 M aqueous solutions of either Cl^- or Br^- . For pure water, 100 % of the U in the outer thin layer is U(VI) after exposure to γ -radiation.

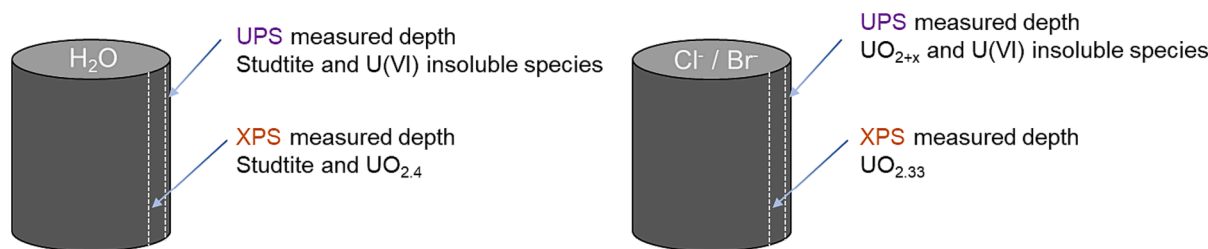


Fig. 10. Summaries of surface compositions after exposure to γ -radiation in pure water and halide solutions at the depth measured by XPS and UPS, respectively.

CRediT authorship contribution statement

Junyi Li: Data curation, Formal analysis, Methodology, Conceptualization, Writing – original draft, Writing – review & editing. **Xianjie Liu:** Investigation, Writing – review & editing. **Mats Jonsson:** Methodology, Funding acquisition, Supervision, Investigation, Conceptualization, Writing – review & editing.

Declaration of competing interest

The authors declare that they have no known competing financial interests or personal relationships that could have appeared to influence the work reported in this paper.

Data availability

Data will be made available on request.

Acknowledgment

The Swedish Nuclear Fuel and Waste Management Company (SKB) [grant numbers 4501747777] and China Scholarship Council (CSC) [grant number 201907930018] are gratefully acknowledged for financial support.

Appendix A. Supplementary material

UO₂ pellet and powder surface pre-washing. Details of volume compensation (normalization) in dissolution experiments. Calibration curve of Br₃⁻ dissolution of UP-2 and UP-3 in pure water and 1 M aqueous solutions of either Cl⁻ or Br⁻ exposed to γ – radiation. Br₃⁻ induced dissolution of UO₂ (for 25 and 75 mg). Mole fraction of U(IV), U(V) and U(VI) from U 4f_{7/2} peaks. Full XPS scans of UO₂ reference sample and the samples after exposures to pure water and 1 M aqueous solutions of either Cl⁻ or Br⁻, respectively. Supplementary data to this article can be found online at <https://doi.org/10.1016/j.apsusc.2023.158955>.

References

- [1] T. Von Berlepsch, B. Haverkamp, Salt as a Host Rock for the Geological Repository for Nuclear Waste, *Elements*. 12 (2016) 257–262.
- [2] SKB. Design and Production of the KBS-3 Repository. Technical Report. TR-10-12. 2010.
- [3] Z. Braden, A. Macfarlane, The Final Countdown to Site Selection for Canada's Nuclear Waste Geologic Repository, *Bull. at. Sci.* 79 (2023) 22–27.
- [4] RWM. Initial Evaluation Report: Theddlethorpe Gas Terminal Site and Surrounding Area within the East Lindsey Area. 2021, 1–26.
- [5] J. Vira, Geological Repository for High-Level Nuclear Waste Becoming Reality in Finland, *Geol. Repos. Syst. Safe Dispos. Spent Nucl. Fuels Radioact. Waste.* (2017) 645–666.
- [6] J. Spinks, *An Introduction to Radiation Chemistry*, 3rd ed., Wiley, New York, 1990.
- [7] E. Ekeröth, O. Roth, M. Jonsson, The Relative Impact of Radiolysis Products in Radiation Induced Oxidative Dissolution of UO₂, *J. Nucl. Mater.* 355 (2006) 38–46.
- [8] C. Nguyen-Trung, G.M. Begun, D.A. Palmer, Aqueous Uranium Complexes. 2. Raman Spectroscopic Study of the Complex Formation of the Dioxouranium(VI) Ion with a Variety of Inorganic and Organic Ligands. 31 (1992) 5280–5287.
- [9] V. Valérie Vallet, U. Wahlgren, I. Grenthe, Probing the Nature of Chemical Bonding in Uranyl(VI) Complexes with Quantum Chemical Methods, *J. Phys. Chem. A*. 116 (2012) 12373–12380.
- [10] J. Li, Z. Szabó, M. Jonsson, Meta-Studtite Stability in Aqueous Solutions. Impact of HCO₃⁻, H₂O₂ and Ionizing Radiation on Dissolution and Speciation, *Dalt. Trans.* 50 (2021) 6568–6577.
- [11] P.L. Zanonato, P. Di Bernardo, Z. Szabó, I. Grenthe, Chemical Equilibria in the Uranyl(vi)-Peroxide-Carbonate System; Identification of Precursors for the Formation of Poly-Peroxometallates, *Dalt. Trans.* 41 (2012) 11635–11641.
- [12] J. Li, Z. Szabó, M. Jonsson, Stability of Studtite in Saline Solution: Identification of Uranyl–Peroxo–Halo Complex, *Inorg. Chem.* 61 (2022) 8455–8466.
- [13] Abrefah, J.; Marschman, S. C.; Jensen, E. D. Examination of the Surface Coatings Removed from K-East Basin Fuel Elements. 1998, PNNL-11806, UC-602.
- [14] C.R. Armstrong, M. Nyman, T. Shvareva, G.E. Sigmon, P.C. Burns, A. Navrotsky, Uranyl Peroxide Enhanced Nuclear Fuel Corrosion in Seawater, *Proc. Natl. Acad. Sci.* 109 (2012) 1874–1877.
- [15] P.C. Burns, R.C. Ewing, A. Navrotsky, Nuclear Fuel in a Reactor Accident, *Science*. 335 (2012) 1184–1188.
- [16] B. Nogrady, Scientists OK Plan to Release One Million Tonnes of Waste Water from Fukushima, *Nature* (2021), <https://doi.org/10.1038/D41586-021-01225-2>.
- [17] W. Men, J. He, F. Wang, Y. Wen, Y. Li, J. Huang, X. Yu, Radioactive Status of Seawater in the Northwest Pacific More than One Year after the Fukushima Nuclear Accident, *Sci. Rep.* 5, No. 7757 (2015).
- [18] N.C. Sturchio, K.L. Kuhlman, R. Yokochi, P.C. Probst, W. Jiang, Z.T. Lu, P. Mueller, G.M. Yang, Krypton-81 in Groundwater of the Culbrea Dolomite near the Waste Isolation Pilot Plant, New Mexico. *J. Contam. Hydrol.* 160 (2014) 12–20.
- [19] S.J. Lambert, Geochemistry of the Waste Isolation Pilot Plant (WIPP) Site, Southeastern New Mexico, U.S.A Appl. Geochem. 7 (1992) 513–531.
- [20] J. Halldin Stenlid, E. Campos dos Santos, R.M. Arán-Ais, A. Bagger, A.J. Johansson, B. Roldan Cuena, J. Rossmeisl, L.G.M. Pettersson, Uncovering the Electrochemical Interface of Low-Index Copper Surfaces in Deep Groundwater Environments, *Electrochimica. Acta.* 362, No. 137111 (2020).
- [21] L.F. Auque, M.J. Gimeno, J.B. Gomez, I. Puigdomenech, J. Smellie, E.L. Tullborg, Groundwater Chemistry around a Repository for Spent Nuclear Fuel over a Glacial, Cycle. TR-06-31 (2006) 1–123.
- [22] F. King, D.S. Hall, P.G. Keech, Nature of the near-Field Environment in a Deep Geological Repository and the Implications for the Corrosion Behaviour of the Container. 52 (2017) 25–30.
- [23] Arcos, D.; Grandia, F.; Doménech Enviros, C. Geochemical Evolution of the near Field of a KBS-3 Repository. 2006, TR-06-16.
- [24] B.G. Ershov, M. Kelm, E. Janata, A.V. Gordeev, E. Bohnert, Radiation-Chemical Effects in the near-Field of a Final Disposal Site: Role of Bromine on the Radiolytic Processes in NaCl-Solutions, *Radiochim. Acta.* 90 (2002) 617–622.
- [25] A. Karim, E. Omar, U. Schmidhammer, B. Rousseau, J. Laverne, M. Mostafavi, Competition Reactions of H₂O^{•+} Radical in Concentrated Cl⁻ Aqueous Solutions: Picosecond Pulse Radiolysis Study, *J. Phys. Chem. A*. 116 (2012) 11509–11518.
- [26] G.G. Jayson, B.J. Parsons, S.A.J. Some, H.R. Simple, Inorganic Chlorine Derivatives in Aqueous Solution. Their Formation Using Pulses of Radiation and Their Role in the Mechanism of the Fricke Dosimeter, *J. Chem. Soc Faraday Trans. 1* (69) (1973) 1597–1607.
- [27] M. Kelm, V. Metz, E. Bohnert, E. Janata, C. Bube, Interaction of Hydrogen with Radiolysis Products in NaCl Solution - Comparing Pulse Radiolysis Experiments with Simulations, *Radiat. Phys. Chem.* 80 (2011) 426–434.
- [28] B.G. Ershov, M. Kelm, A.V. Gordeev, E. Janata, A Pulse Radiolysis Study of the Oxidation of Br⁻ by Cl₂⁻ in Aqueous Solution: Formation and Properties of ClBr⁻, *Phys. Chem. Chem. Phys.* 4 (2002) 1872–1875.
- [29] V. Metz, A. Loida, E. Bohnert, D. Schild, K. Dardenne, Effects of Hydrogen and Bromide on the Corrosion of Spent Nuclear Fuel and γ -Irradiated UO₂(s) in NaCl Brine, *Radiochim. Acta.* 96 (2008) 637–648.
- [30] S. Sundin, B. Dahlgren, O. Roth, M. Jonsson, H₂O₂ and Radiation Induced Dissolution of UO₂ and SIMFUEL in HCO₃⁻ Deficient Aqueous Solution, *J. Nucl. Mater.* 443 (2013) 291–297.
- [31] A. Barreiro Fidalgo, Y. Kumagai, M. Jonsson, The Role of Surface-Bound Hydroxyl Radicals in the Reaction between H₂O₂ and UO₂, *J. Coord. Chem.* 71 (2018) 1799–1807.
- [32] J. Li, X. Liu, M. Jonsson, Exploring the Change in Redox Reactivity of UO₂ Induced by Exposure to Oxidants in HCO₃⁻ Solution, *Inorg. Chem.* 62 (2023) 7413–7423.
- [33] J.M. Joseph, B.S. Choi, P. Yakabuskie, J.C. Wren, A Combined Experimental and Model Analysis on the Effect of PH and O₂(Aq) on γ -Radiolytically Produced H₂ and H₂O₂, *Radiat. Phys. Chem.* 77 (2008) 1009–1020.

- [34] K. Hata, H. Inoue, T. Kojima, A. Iwase, S. Kasahara, S. Hanawa, F. Ueno, T. Tsukada, Hydrogen Peroxide Production by Gamma Radiolysis of Sodium Chloride Solutions Containing a Small Amount of Bromide Ion, *Nucl. Technol.* 193 (2016) 434–443.
- [35] M. Mirdamadi-Esfahani, I. Lampre, J.L. Marignier, V. de Waele, M. Mostafavi, Radiolytic Formation of Tribromine Ion Br³⁻ in Aqueous Solutions, a System for Steady-State Dosimetry, *Radiat. Phys. Chem.* 78 (2009) 106–111.
- [36] B.G. Ershov, A.V. Gordeev, E. Janata, M. Kelm, Radiation-Chemical Oxidation of Bromide Ions and Formation of Tribromide Ions in Weakly Acidic Aqueous Solutions, *Mendeleev Commun.* 11 (2001) 149–150.
- [37] P.K. Adanuvor, R.E. White, S.E. Lorimer, The Effect of the Tribromide Complex Reaction on the Oxidation/ The Effect of the Tribromide Complex Reaction on the Oxidation/ Reduction Current of the Br²/Br⁻ Electrode Reduction Current of the Br²/Br⁻ Electrode, *J. Electrochem. Soc.* 1450–1454 (1987).
- [38] **Standard Reduction Potentials.** <https://www.av8n.com/physics/redpot.htm>.
- [39] I. Lampre, J.L. Marignier, M. Mirdamadi-Esfahani, P. Pernot, P. Archirel, M. Mostafavi, Oxidation of Bromide Ions by Hydroxyl Radicals: Spectral Characterization of the Intermediate BrOH•-, *J. Phys. Chem. A.* 117 (2013) 877–887.
- [40] G. El Jamal, J. Li, M. Jonsson, H₂O₂-Induced Oxidative Dissolution of UO₂ in Saline Solutions, *Eur. J. Inorg. Chem.* 2021 (2021) 4175–4182.
- [41] M. Olsson, A.M. Jakobsson, Y. Albinsson, Surface Charge Densities of Two Actinide (IV) Oxides: UO₂ and ThO₂, *J. Colloid Interface Sci.* 256 (2002) 256–261.
- [42] A. Husain, Charge Development at the Uranium Oxide-Solution Interface, *J. Colloid Interface Sci.* 102 (1984) 389–399.
- [43] J. Li, L. Li, M. Jonsson, Ecotoxicology and Environmental Safety Formation and Stability of Studtite in Bicarbonate-Containing Waters, *Ecotoxicol. Environ. Saf.* 263 (2023), 115297.
- [44] G. El Jamal, T. Gouder, R. Eloirdi, M. Jonsson, Monitoring the Gradual Change in Oxidation State during Surface Oxidation or Reduction of Uranium Oxides by Photoemission Spectroscopy of the 5f States, *J. Nucl. Mater.* 560 (2022), 153504.
- [45] K.I. Maslakov, Y.A. Teterin, A.J. Popel, A.Y. Teterin, K.E. Ivanov, S.N. Kalmykov, V. G. Petrov, R. Springell, T.B. Scott, I. Farnan, XPS Study of the Surface Chemistry of UO₂ (111) Single Crystal Film, *Appl. Surf. Sci.* 433 (2018) 582–588.
- [46] S.B. Donald, Z.R. Dai, M.L. Davison, J.R. Jeffries, A.J. Nelson, An XPS Study on the Impact of Relative Humidity on the Aging of UO₂ Powders, *J. Nucl. Mater.* 487 (2017) 105–112.
- [47] N.L. Hansson, P.L. Tam, C. Ekberg, K. Spahiu, XPS Study of External α -Radiolytic Oxidation of UO₂ in the Presence of Argon or Hydrogen, *J. Nucl. Mater.* 543 (2021), 152604.
- [48] G. El Jamal, T. Gouder, R. Eloirdi, E. Tereshina-Chitrova, L. Horádk, M. Jonsson, Mixed H₂O/H₂ Plasma-Induced Redox Reactions of Thin Uranium Oxide Films under UHV Conditions, *Dalt. Trans.* 50 (2021) 12583–12591.
- [49] M. Schindler, F.C. Hawthorne, M.S. Freund, P.C. Burns, XPS Spectra of Uranyl Minerals and Synthetic Uranyl Compounds. I: The U 4f Spectrum, *Geochim. Cosmochim. Acta.* 73 (2009) 2471–2487.
- [50] E.S. Ilton, P.S. Bagus, XPS Determination of Uranium Oxidation States, *Surf. Interface Anal.* 43 (2011) 1549–1560.
- [51] G. Heisbourg, S. Hubert, N. Dacheux, J. Purans, Kinetic and Thermodynamic Studies of the Dissolution of Thoria-Urania Solid Solutions, *J. Nucl. Mater.* 335 (2004) 5–13.
- [52] Y.A. Teterin, A.J. Popel, K.I. Maslakov, A.Y. Teterin, K.E. Ivanov, S.N. Kalmykov, R. Springell, T.B. Scott, I. Farnan, XPS Study of Ion Irradiated and Unirradiated UO₂ Thin Films, *Inorg. Chem.* 55 (2016) 8059–8070.
- [53] T. Vitova, I. Pidchenko, S. Biswas, G. Beridze, P.W. Dunne, D. Schild, Z. Wang, P. M. Kowalski, R.J. Baker, Dehydration of the Uranyl Peroxide Studtite, [UO₂(N₂-O₂)(H₂O)₂·2H₂O], Affords a Drastic Change in the Electronic Structure: A Combined X-Ray Spectroscopic and Theoretical Analysis, *Inorg. Chem.* 57 (2018) 1735–1743.
- [54] M. Fairley, N.M. Myers, J.E.S. Szymanowski, G.E. Sigmon, P.C. Burns, J.A. Laverne, Stability of Solid Uranyl Peroxides under Irradiation, *Inorg. Chem.* 58 (2019) 14112–14119.
- [55] J. Li, A.C. Maier, M. Jonsson, Stability of Studtite in Aqueous Suspension: Impact of HCO₃⁻ and Ionizing Radiation on the Dynamics of Dissolution, *ACS Appl. Energy Mater.* 3 (2020) 352–357.